

# Quaternary adaptive optics

MANUEL P. CAGIGAL,<sup>1,\*</sup> ANTONIO FUENTES,<sup>1</sup> MIGUEL A. CAGIGAS,<sup>2</sup> PEDRO J. VALLE,<sup>1</sup>  XESÚS PRIETO-BLANCO,<sup>3</sup>  AND VIDAL F. CANALES<sup>1</sup> 

<sup>1</sup>*Departamento de Física Aplicada, Universidad de Cantabria, 39005 Santander, Spain*

<sup>2</sup>*Instituto de Astrofísica de Canarias, Vía Láctea s/n, 38200 La Laguna, Spain*

<sup>3</sup>*Facultade de Óptica e Optometría, Campus Vida, E-15782 Santiago de Compostela, Spain*

\*[perezcm@unican.es](mailto:perezcm@unican.es)

**Abstract:** We present a new Point Diffraction Interferometer (PDI). Binary adaptive optics (BAO) and Quaternary Adaptive Optics (QAO) can be performed with the help of this PDI as a wavefront sensor. The PDI interferogram, once binarized, is used in two consecutive steps to produce a quaternary mask with phase values  $0$ ,  $\pi/2$ ,  $\pi$  and  $3\pi/2$ . The addition of the quaternary mask compensates for the aberrated wavefront and allows us to reach a Strehl ratio of about 0.81. We have verified through computer simulations that the use of QAO depends on the number of actuators of the compensating device to achieve effective compensation. The technique was successfully validated through an experiment.

© 2019 Optical Society of America under the terms of the [OSA Open Access Publishing Agreement](#)

## 1. Introduction

The propagation of light through the atmosphere results in phase aberrations in the wave that severely reduce the resolution of ground-based imaging systems. Adaptive optics (AO) systems reduce the roughness of the incoming distorted wavefront by adding different phase values at specific points on the distorted wavefront. However, in practice, this simple concept is difficult to implement, and adaptive optics systems cannot yet reach their theoretical performance limit. In addition, the next generation of large telescopes poses a new challenge, given that the peak-to-valley distance on the distorted wavefront can take huge values. Binary adaptive optics (BAO) is based on the use of binary phase masks, to perform a half-wave correction in the distorted field. The technique was introduced in the early 90s [1,2] and since then different analyses have been carried out to demonstrate its viability [3,4]. Moreover, it has been considered for application to optical tweezers [5] and laboratory phase screen generation [6]. Its main advantage is simplicity, although the maximum achievable Strehl ratio is around 0.4. To overcome this limitation, it is possible to perform additional compensations such as quarter-wave compensation, or quaternary adaptive optics (QAO), eighth-wave compensation, or octary adaptive optics (OAO), etc.

Until now, quarter-wave adaptive optics has been theoretically analyzed and some experiments based on the use of a Smartt interferometer at harmonics wavelengths have been proposed [2]. However, as far as we know, no experimental measurements have been carried out except half-wave compensation. In this paper, we propose a two-step technique to achieve half and quarter-wave compensations. The proposed technique is very simple, given that the two steps can be carried out using a point diffraction interferometer (PDI) as wavefront sensor. In the first step, a half-wave correction is introduced as in BAO. Then, the half-wave compensated wavefront is sensed to obtain a quarter-wave mask. The quarter-wave mask is added to the half-wave mask obtained in the first step and the total mask is used to perform the QAO compensation.

Compensation techniques based on discrete phase values have several advantages compared to other techniques; firstly they use a PDI wavefront sensor, which is easy to manufacture and implement, secondly, they do not need any algorithm to reconstruct the wavefront surface and, finally, their dynamic range is infinite, which is particularly interesting for extremely large

telescopes. Their main drawbacks are that these techniques can only achieve their maximum performances when the number of actuators in the compensator device is sufficiently large.

In this paper, we present a general review of QAO, then describe the characteristics for the PDI to be useful for the quarter-wave compensation. Next, we perform a theoretical complementary analysis of this technique using a computer simulation and finally carry out an experimental verification of the BAO and QAO techniques.

## 2. Quaternary adaptive optics

The strategy followed by standard adaptive optics (AO) is to measure the local phase distortion and to use a phase device, usually a deformable mirror, to increase or reduce the local phase of the distorted wavefront as a way to improve the final image quality. In contrast to this strategy, Binary Adaptive Optics consists in introducing a phase retardation of 0 or  $\pi$  at some points of the wavefront [1]. This technique is simpler and faster than the AO. The strategy of QAO is the same as that of BAO but it introduces four different phase retardation values (0,  $\pi$ ,  $\pi/2$  and  $3\pi/2$ ). According to the expression for the achievable Strehl ratio [1] as a function of the phase interval  $\Delta\phi$  in which the wavefront is contained:

$$S = \text{sinc}^2\left(\frac{\Delta\phi}{2}\right) \quad (1)$$

The maximum Strehl ratio achievable by BAO is 0.4. This value increases to 0.81 for QAO compensation. Additional compensation such as OAO, could increase this value to 0.94. Given that increasing the compensation level increases the difficulty of providing good compensation, we will first analyze the BAO and QAO compensation process. In the next paragraph, we explain a simple procedure to obtain the phase mask required for an efficient QAO compensation.

### 2.1. QAO compensation

Both the BAO and QAO techniques are based on the use of the PDI as a wavefront sensor. The PDI is a common-path interferometer that has the advantage of being simple, cheap and robust [7,8]. The scheme of the PDI sensor is shown in Fig. 1. The distorted wavefront located on the entrance pupil of the optical system at a distance equal to the focal length of lens L1 is focused by lens L1 onto a mask (M). The mask has a small central area with transmittance or phase different to the rest of the mask. The central area creates a reference wavefront, which interferes with rest of the wavefront thanks to lens L2. The resulting interference pattern is detected by a camera placed in the L2 focal plane, which is conjugated to that of the system's pupil. Despite its simplicity, this sensor is not widely used because it is difficult to recover phase values that describe the wavefront, except in some particular cases. However, this sensor is very appropriate for BAO and QAO compensation since it enables us a direct recovery of the phase information needed.

In the BAO technique, a part of the incoming distorted wavefront (DW) is sent to the PDI sensor with the help of a beam splitter (BS) and an auxiliary mirror (Mr) as shown in Fig. 2. The detected interferogram in the PDI camera is used to create a binary phase mask by assigning a phase of  $\pi$  to those pixels whose intensity is above a threshold. Other pixels are assigned to zero phase. Then, this binary function (BF1) is added to the distorted wavefront with the help of a spatial light modulator (SLM) to compensate the incoming wavefront, which produces a wavefront that, once wrapped, is in the range of  $0-\pi$ .

To obtain a quaternary compensating function, the process is repeated. The compensated wavefront (BCW) forms a new interferogram on the PDI camera. The new interferogram is binarized to assign a phase of  $\pi/2$  to pixels whose intensity is over a threshold whilst other pixels remain at zero phase. The new  $0-\pi/2$  binary function (BF2) is added to the first one (BF1)

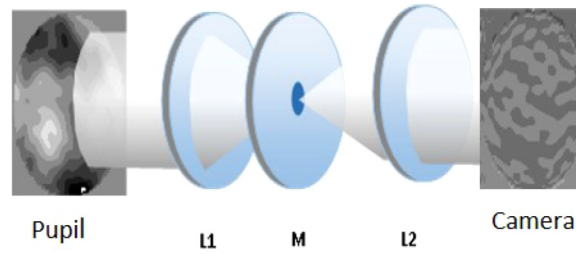


**Fig. 1.** The PDI sensor consists of a 4- $f$  system, formed by lenses L1 and L2, and a mask placed in the common focus plane (M). A camera placed after lens L2 records the interference pattern produced by the mask.

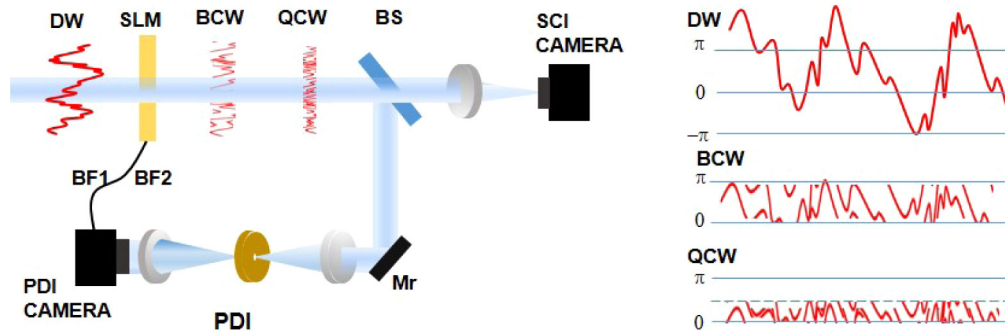


**Fig. 2.** Scheme of operation of QAO technique. The first step is like in BAO. The binarization of the interferogram produces a binary phase mask, BF1, which added to the distorted wavefront DW produces the BAO compensated wavefront, BCW. This wavefront generates a new interferogram used to create a new binary phase mask, BF2. The QAO compensation consist of the addition of BF1 + BF2 to the DW to create the quaternary compensated wavefront QCW.

resulting in a quaternary phase mask, BF1 + BF2, with values  $0, \pi/2, \pi$  and  $3\pi/2$ . When the quaternary phase mask is added to the former distorted wavefront, we obtain a new wavefront (QCW) with phase values contained in the  $0 - \pi/2$  range. The key element in successfully performing BAO and QAO compensations is the mask M. To perform BAO compensation, we can use any kind of mask, given that it provides a reference wavefront and an aberrated one. However, to carry out QAO compensation, the reference wavefront provided by the mask must have a difference in phase close to  $\pi/2$  with respect to the aberrated one.

## 2.2. Two-step compensating process

Let us consider the field at the entrance pupil of the optical system described by  $A_{x,y} \exp(-i\phi_{x,y})$ . The distorted wavefront, DW, is described by the phase function  $\phi_{x,y}$ . We can model the intensity of the interferogram recorded in the first step by the sum of two fields:

$$I_{x,y} = |A_{x,y} \exp(-i\phi_{x,y}) + A_0 \exp(-i\phi_0)| \quad (2)$$

where  $A_0 \exp(-i\phi_0)$  is the reference field created by the mask of the PDI at the camera plane. Note that  $\phi_0$  is the phase of the reference wave at this plane. From Eq. (2) it is easy to obtain (assuming  $A_{x,y} = A_0$ ):

$$\cos(\phi_{x,y} - \phi_0) = \frac{I_{x,y}}{2|A_{x,y}|^2} - 1 \quad (3)$$

We obtain the binary compensating function (BF1) as:

$$\text{BF1}_{x,y} = \begin{cases} 0 & \text{if } \cos(\phi_{x,y} - \phi_0) \geq 0 \\ \pi & \text{if } \cos(\phi_{x,y} - \phi_0) < 0 \end{cases} \quad (4)$$

From the binary function,  $\text{BF1}_{x,y}$  we obtained the sign mask:

$$\text{SM1}_{x,y} = \begin{cases} 1 & \text{if } \text{BF1}_{x,y} = 0 \\ -1 & \text{if } \text{BF1}_{x,y} = \pi \end{cases} \quad (5)$$

To compensate the incoming distorted field  $A_{x,y} \exp(-i\phi_{x,y})$  it is enough to multiply the distorted field by the sign mask  $\text{SM1}_{x,y}$ . The resulting binary compensated wavefront will be:

$$\text{BCW}_{x,y} = \text{SM1}_{x,y} A_{x,y} \exp(-i\phi_{x,y}) = A_{x,y} \exp(-i\phi'_{x,y}) \quad (6)$$

In the BAO technique, the compensation process would stop here. However, in the QAO, the compensated field obtained after the first iteration, BCW, is sensed by the PDI once again. Note that the reference field,  $A_0 \exp(-i\phi'_0)$ , is different from that of the first step. A threshold is applied to the resulting interferogram and a new binary function with step  $\pi/2$  is obtained:

$$\text{BF2}_{x,y} = \begin{cases} 0 & \text{if } \cos\left(\phi'_{x,y} - \phi'_0 - \frac{\pi}{2}\right) = \sin(\phi'_{x,y} - \phi'_0) \geq 0 \\ \frac{\pi}{2} & \text{if } \cos\left(\phi'_{x,y} - \phi'_0 - \frac{\pi}{2}\right) = \sin(\phi'_{x,y} - \phi'_0) < 0 \end{cases} \quad (7)$$

To produce a new function:

$$\text{SM2}_{x,y} = \begin{cases} 1 & \text{if } \text{BF2}_{x,y} = 0 \\ i & \text{if } \text{BF2}_{x,y} = \frac{\pi}{2} \end{cases} \quad (8)$$

where in Eq. (7) we have clearly included the required extra  $\pi/2$  phase of the PDI mask.

The resulting quaternary compensated wavefront is:

$$\text{QCW}_{x,y} = \text{SM2}_{x,y} \text{SM1}_{x,y} A_{x,y} \exp(-i\phi_{x,y}) = A_{x,y} \exp(-i\phi'_{x,y}) \quad (9)$$

The field of Eq. (9), once wrapped, is in the range  $0 < \phi'_{x,y} < \pi/2$ . According to Eq. (1), the QAO technique will provide a Strehl ratio  $S \approx 0.81$  for fully developed turbulence, which, together with the low requirements for the wavefront sensor and compensator, the simplicity of the phase retrieval algorithm and the short delay between sensing and compensation, make QAO a competitive alternative to the AO technique.

To check the viability of the process, we carried out a computer simulation. As an example, Fig. 3 shows a comparison between a binary mask obtained from a direct binarization of the incoming distorted wavefront (a) and the corresponding one obtained using Eq. (4) (b). It can be seen that, although they are not identical, there is great similarity between the two phase masks. We also observe the similarity between the mask obtained from the direct discretization into four levels of the aberrated wavefront (c) and that corresponding to the addition of the two binary masks obtained during the QAO compensation process, Eqs. (4) and (7) (d).

In this paper, we have only dealt with static aberrations. Nevertheless, when the system is working in closed-loop, it would be enough to perform BAO compensation once, and then to repeat the QAO compensation. In any case, the compensation process has to take a shorter time than the coherence time of atmospheric evolution. In these conditions, the QAO compensation becomes as easy and fast as the BAO one.

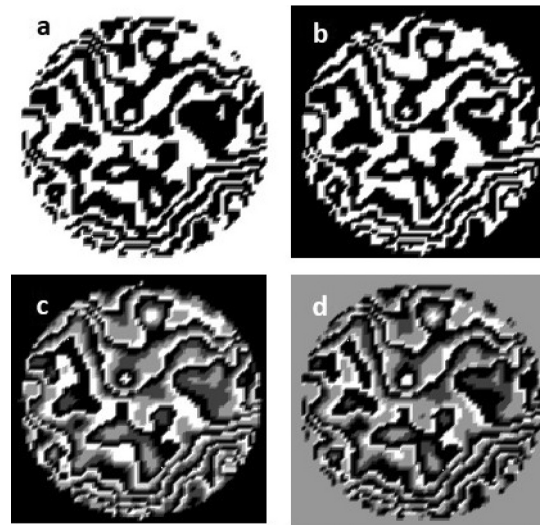


**Fig. 3.** Comparison between the direct binarization of the wavefront at the entrance pupil of the optical system (a) and the binary wavefront resulting from the PDI sensor (b). Quaternary function obtained from the direct discretization of the aberrated wavefront into four levels (c) and that obtained after binarizing the two interferograms obtained during the QAO compensation process (d).

### 3. QAO performance analysis

The performance analysis of the BAO and QAO was carried out by computer simulation. A series of phase screens  $\phi_{x,y}$  were simulated following the Kolmogorov statistics. Then the corresponding electric field was calculated  $A_{x,y} \exp(-i\phi_{x,y})$ , where the amplitude  $A$  is constant and equal to 1. A wavefront sensor such as the one in Fig. 1 was simulated taking advantage of the Fast Fourier Transform (FFT). We used a PDI mask with constant phase and a difference in phase of  $\pi/2$  in the central area. The PDI interferogram was used to compensate the corresponding distorted wavefront as shown by Eq. (6) for BAO and Eq. (9) for QAO. Then, the compensated image was obtained as the Fourier transform of Eq. (6) for BAO and Eq. (9) for QAO. Different aspects of the BAO technique have already been analyzed [1,2,6] and can be easily extrapolated to QAO. Moreover, an analysis of the QAO chromatic and fitting errors dependence has already been carried out by G.D. Love et al. [2]. However, there is an important difference between the two techniques with respect to the number of actuators required.

#### 3.1. Effect of the number of actuators

Given that, the size of the Fried parameter corresponds to an area in which the phase variation is smaller than 1 rad and that, for example, the BAO only acts in those areas in which the difference in phase is larger than  $\pi$  rad, it seems that the numbers of pixels required for the compensating device could be low. We carried out an analysis of the effect of the pixel size of the compensating device on the compensation capability of the system. We used distorted wavefronts with  $D/r_0$  values of 10, 20 and 40, where  $D$  is the entrance pupil diameter and  $r_0$  is the Fried parameter. We started with a pixel size small enough to allow the system to reach the highest possible Strehl values.

Figure 4 shows the Strehl ratio attainable by BAO as a function of the compensating device pixel size expressed in  $r_0$  units for different  $D/r_0$  values. A good compensation can be achieved even when the pixel size of the compensating device is close to  $r_0$ . In particular, for  $D/r_0 = 40$  the

maximum possible Strehl is achieved for an actuator size of about  $r_0/2$ , whilst for  $D/r_0 = 10$  an actuator size of about  $1.25r_0$  is sufficient to achieve the maximum possible Strehl ratio. Hence, as  $D/r_0$  increases, a higher sampling rate is required from the compensating device in order to achieve the highest possible degree of compensation. This result is particularly interesting for extremely large telescopes where  $D/r_0$  takes high values and proper sampling in the compensating device becomes crucial.

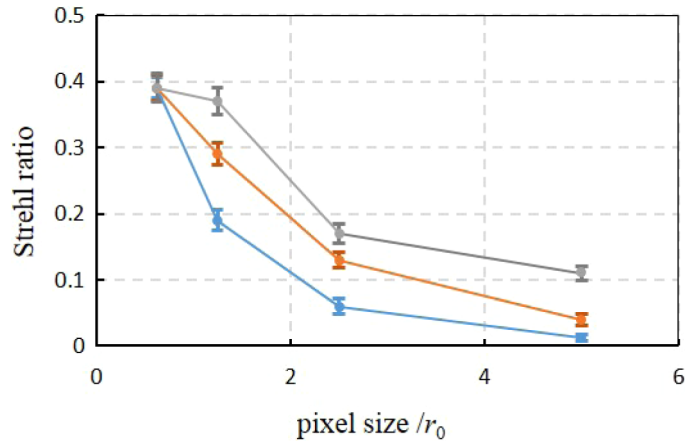


**Fig. 4.** Strehl ratio attainable by BAO as a function of the compensating device pixel size expressed in  $r_0$  units for  $D/r_0 = 40$  (blue line), 20 (orange line) and 10 (grey line).

We also carried out a comparison between the Strehl achievable for BAO and QAO as a function of the pixel size of the compensating device. We started using a pixel small enough to allow both techniques to reach their maximum Strehl value. Then, the compensating process was repeated, but binning the pixels of the compensator device. Figure 5 shows the Strehl reached when applying BAO and QAO according to the degree of binning. A binning value of  $n$  means that a binned pixel contains  $n \times n$  initial pixels.

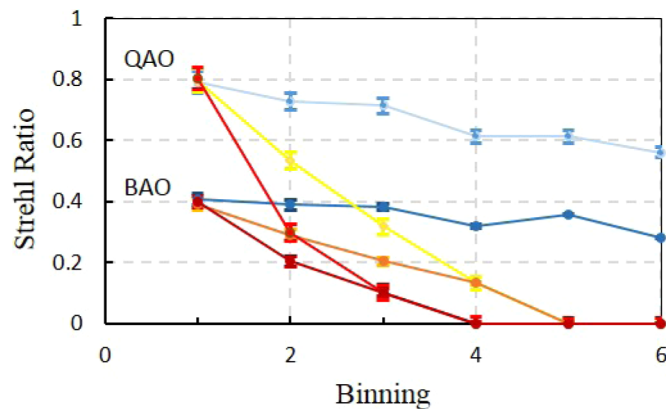


**Fig. 5.** Strehl ratio attained by the BAO and QAO systems as a function of the binning applied to the pixels of the compensating device for different  $D/r_0$  values.  $D/r_0 = 5$ : light blue and dark blue lines,  $D/r_0 = 20$ : light yellow and dark yellow lines and  $D/r_0 = 40$ : light red and dark red lines.

Figure 5 shows that the Strehl ratio attainable by the BAO and QAO systems are those expected when the pixel size of the compensating device is small enough,  $S = 0.4$  for BAO and  $S = 0.8$

for QAO. When compensating device pixels are binned, the Strehl ratio of both QAO and BAO decreases quickly. An interesting result is that, as the Strehl ratio provided by QAO decreases faster than that of the BAO, for a particular binning level QAO and BAO provide the same compensation degree and the same Strehl ratio. The binning level in which QAO and BAO perform similarly is lower for high  $D/r_0$  values, as could be expected. Other interesting behavior is that for low  $D/r_0$  values the attainable compensation degree is only slightly affected by binning.

### 3.2. Errors in the compensation

The BAO and QAO compensation processes may be affected by different errors: errors involved in the interferogram detection, errors in the interferogram binarization process and errors affecting the compensating device. G.D. Love et al. in [2] show the analysis of the effect of the detecting broadband sources on the Strehl values for BAO and QAO, and also demonstrate how the number of detected photons per correction element may affect the attainable Strehl ratio. Next, we will analyze errors affecting the binarization process. The binarization of an interferogram can be accomplished following different procedures. There are different techniques to extract a binary map starting from an interferogram [9,10]. Considering that the interferogram intensity is given by Eq. (2), the maximum  $I_M$  and minimum  $I_m$  intensity values recorded in the interferogram will be:

$$\begin{aligned} I_M &= |A_{x,y}|^2 + |A_0|^2 + 2|A_{x,y}||A_0| \\ I_m &= |A_{x,y}|^2 + |A_0|^2 - 2|A_{x,y}||A_0| \end{aligned} \quad (10)$$

The condition for an effective binarization is that half of the peak-to-valley distance is greater than the typical deviation of the detection noise,  $\sigma_n$ :

$$\frac{I_M - I_m}{2} = 2|A_{x,y}||A_0| > \sigma_n \quad (11)$$

The detection noise comprises the electronic, or readout, noise and the shot noise. We will consider readout noise to be negligible compared to the dominant shot noise. Given the Poissonian nature of the shot noise, its typical deviation is the square root of the mean intensity reaching the pixel. According to Eq. (10) the condition for an effective binarization becomes:

$$2|A_{x,y}||A_0| > \sqrt{|A_{x,y}|^2 + |A_0|^2} \quad (12)$$

Obviously, this inequality depends on the magnitude of the amplitude of the reference wave,  $A_0$ . For strongly aberrated wavefronts, the energy inside the central area of the PDI will be small and Eq. (12) will be fulfilled only for a limited number of points. This problem can be solved by repeating the BAO process many times in order to gradually increase the energy of the reference wavefront and make  $|A_0|$  comparable to  $|A_{x,y}|$ , as shown in [11]. An additional problem derives from the lack of flatness of the reference wavefront. To solve this problem in a simple way, it is enough to apply an adaptive local threshold over the interferogram image, as we will show in the next section. The area used to determine the threshold must be adjusted to achieve an optimum result and it depends on the flatness of the reference wave. However, this process is fast and an optimum area value is quickly achieved for a particular interferometric set-up.

## 4. Experimental checking

### 4.1. Experimental set-up and procedure

Different analyses have been carried out in the context of binary compensation. Some of them were oriented to binary phase compensation using a SLM [12] or a deformable mirror [4] and others to binary amplitude modulation [13]. We carried out an experiment reproducing the

results of previous experiments on binary phase compensation (half-wave compensation) and we extended the technique to quarter-wave compensation. The set-up we used is based on the Thorlabs kit AOK2, which is shown in Fig. 6. The light source is a laser diode (635 nm) which illuminates a micro-electro-mechanical deformable mirror (DM) with 32 active actuators (Thorlabs DM32-35-Ux01). After the mirror, the light reaches a SLM (Hamamatsu X8267-16) and then it is sent to a Shack-Hartmann (SH) wavefront sensor (Thorlabs WS150-SC) and to a PDI wavefront sensor. The PDI consists of a 4- $f$  system with a mask  $M$  (see Fig. 3) placed on the intermediate common focus plane. A pellicle beam splitter sends part of the energy to the camera (SC) to form the compensated image. We placed a mirror, SLM and sensors on planes conjugated to that of the pupil plane with the help of a series of 4- $f$  systems built with pairs of achromatic lenses.

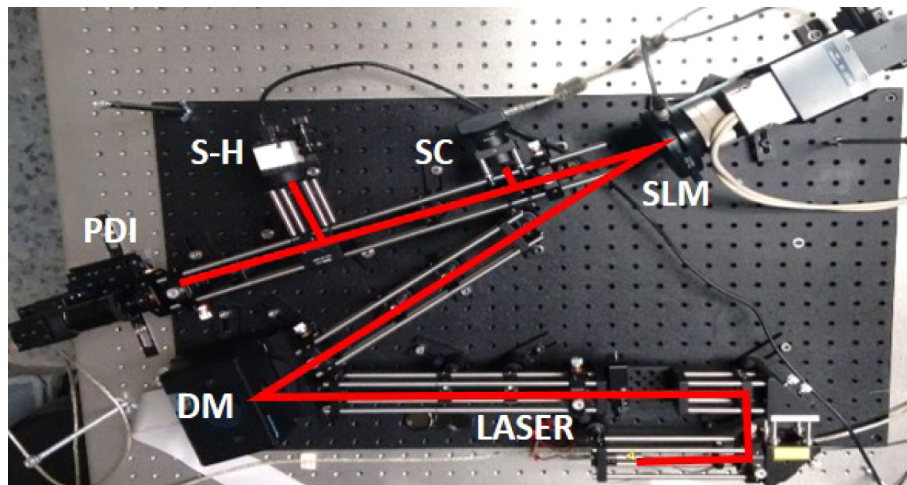


**Fig. 6.** Experimental set-up.

The deformable mirror introduces a wavefront distortion which is simultaneously measured by the SH and the PDI wavefront sensors. The BAO compensation is based on the binarization of the PDI interferogram. The interferogram was binarized using the local average intensity as a threshold, which has been estimated over an area of 20-pixels radius. Then, once scaled, it was sent to the SLM to compensate the distortion introduced by the mirror. To achieve QAO compensation, we repeated the same procedure but this time the threshold was estimated with an area of 5-pixels radius.

We used two different masks  $M$ . The first was a transmittance mask consisting of a thin chrome film, with thickness of approximately  $\lambda/10$  (61 nm) coated on a transparent glass substrate with a central hole of 7  $\mu\text{m}$ . The thin chrome film creates a semitransparent region around the central hole. It is important to bear in mind that this mask not only affects the amplitude of the incoming field but also its phase. The refraction index of chrome for the 635 nm red laser light is around 3.3, which introduces a phase retardation of about  $0.44\pi$  with respect to the field that passes through the central hole. In addition, we use a phase mask consisting of flat glass with an additional cylindrical phase element of diameter about  $2 \lambda/D$ . The cylindrical element presents a difference in phase with respect to the flat glass of  $\pi/2$ . The phase element was manufactured for performing this experiment, at the Universidad de Santiago de Compostela.

The phase mask was fabricated by silver/sodium ion exchange on soda-lime plate glass containing an aluminium mask on one of its faces. A two-stage photolithographic method was used to obtain the mask. First, some flat glass substrates were one-side aluminium coated in a high vacuum deposition chamber until a 0.3  $\mu\text{m}$  thick layer was obtained; then we deposited a

layer of photoresist on the aluminum one by spin coating. At the same time, we printed a 3.92 mm diameter black disk on glossy paper and we photoreduced it on one of the coated substrates to obtain an intermediate mask. For that, we used a Linhof enlarger provided with a Schneider Xenon-Sapphire 4.5/95 objective working at a magnification of about  $-0.075$  and using its full aperture to optimize the resolution at the center of the field. The original was illuminated with four commercial 125-W Hg lamps each and the substrate was exposed for 2 hours. After developing the photoresin, etching the aluminum layer and removing the residual photoresin, an aluminum disk on a transparent substrate was obtained. This intermediate mask was photoreduced again in a similar way (second stage). However, this time the illumination was done by transmission with a Khoeler-type system which consisted of a lens before the intermediate mask that marked an image of only one mercury lamp in the input pupil of the Schneider objective. The exposure lasted 15 min, to obtain as a final mask an aluminium disk having a diameter of  $24\ \mu\text{m}$ . Similarly, an aluminum disk of  $18\ \mu\text{m}$  in diameter was also fabricated.

These masked glass plates were immersed in a molten mixture of sodium and silver nitrate salts. In this process, the silver cations diffuse into the glass and replace those of sodium which form salt. Thus, a very uniform exchanged layer is formed having a decreasing silver concentration from the surface to the interior of the substrate. The thickness of this layer increases with time, and the penetration become faster as temperature increases. Since the refractive index of the glass increases proportionally to the silver concentration, a gradient index layer is formed. However, the aluminum mask prevents the silver cations from crossing the glass surface, so no index change appears under the mask. After the ion exchange process, the aluminium mask is removed. When this sample is normally illuminated with a plane wave, the part of the wavefront that crosses the exchanged layer acquires an extra phase with respect to the part crossing the unchanged glass; so the emerging wave is no longer a plane wave. Following the Montero-Orille [14] procedure we achieve an inaccuracy lower than  $\lambda/100$  for a  $\pi/2$  phase plate. The main limitation of the ion exchange for fabricating phase plates arises from the lateral diffusion under the edge of the mask, which limits the lateral resolution of the element to a few  $\mu\text{m}$ ; a value similar to that of the penetration depth. Figure 7 is a differential interference contrast (DIC) microscopic image of the  $24\text{-}\mu\text{m}$  diameter element that can be used in a point diffraction interferometer. The image shows a pseudo three-dimensional representation of the generated phase. We can see a circular plateau bounded by a phase ramp of about  $5\ \mu\text{m}$  wide.

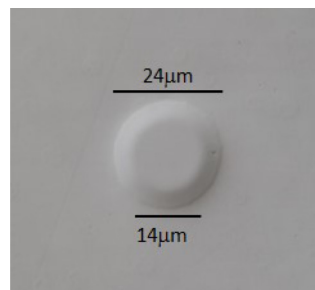


**Fig. 7.** DIC microscopic image of the  $24\text{-}\mu\text{m}$  diameter phase element to be used in the PDI.

#### 4.2. Experiment results

In this section, we detail some of the results obtained using BAO and QAO with the help of the experimental set-up in Fig. 6. We checked the Strehl ratio and the interferogram residual phase variance with and without distortion, and for the two levels of compensation. The process was repeated for different kinds of distortions and for different distortion degrees. As an example,

we started by checking simple aberrations corresponding to individual Zernike polynomials. Figure 8(a) shows the interferogram detected by the PDI camera corresponding to a wavefront affected by positive defocus (about  $6\pi$  phase error). To obtain the binary ( $0-\pi$ ) mask, a threshold was applied to this interferogram and it was binarized and scaled. The resulting binary mask, named BF1 in Eq. (3) is shown in Fig. 8(b). This mask was then used to compensate the distorted wavefront. The compensated wavefront produces a new interferogram shown in Fig. 8(c). Once again, a threshold was applied to this compensated interferogram and it was binarized and scaled to obtain a binary mask taking values 0 and  $\pi/2$ , BF2. This function is shown in Fig. 8(d). The quaternary mask (QAO mask) shown in Fig. 8(f) was obtained by adding Figs. 8(b) and 8(d). Once the QAO mask was applied, the new compensated interferogram shown in Fig. 8(e) was obtained.

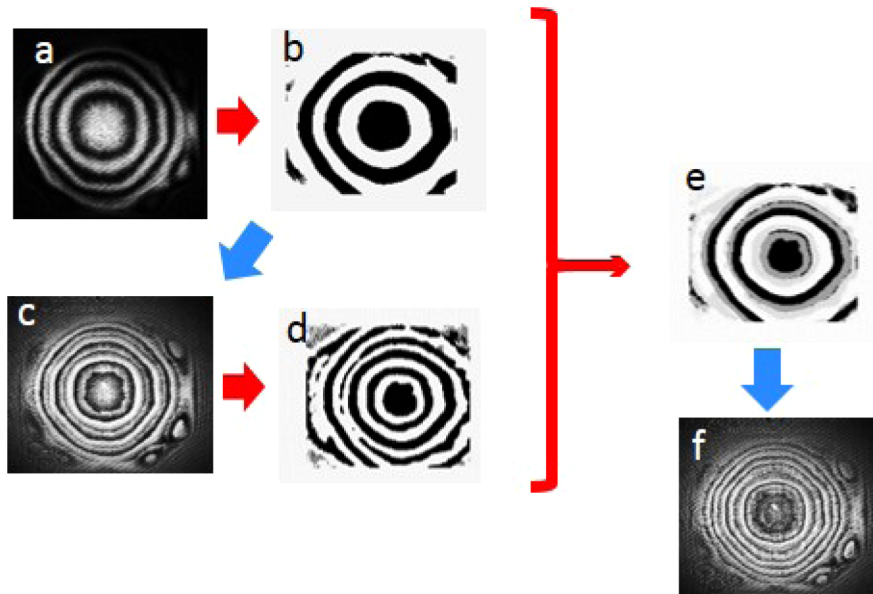


**Fig. 8.** (a) Interferogram of the distorted wavefront. (b) Binary function BF1 obtained from Fig. 8(a), (c) Interferogram of the BF1 compensated wavefront, (d) Binary function BF2 obtained from Fig. 8(c), (e) Quaternary function BF1 + BF2 obtained from Fig. 8(b) + 8(d), (f) Interferogram of the QAO compensated wavefront.

The same procedure was repeated for different Zernike polynomial aberrations obtaining similar results. We also checked the technique with randomly distorted wavefronts. Figure 9 shows the same sequence as that of Fig. 8 but for the case of a random distortion. There is an important difference between these two cases. We see that the highly aberrated wavefront in Fig. 9 shows short-term ripples and small areas of constant phase. To achieve efficient compensation, the number of actuators required was greater than that required to compensate the aberration shown in Fig. 8, as expected after the analysis shown in Fig. 5.

As an example of the technique's performance, Fig. 10 shows transverse cuts of the PSF intensity for the plane wavefront used as a reference (black line), the aberrated wavefront (yellow line), the BAO compensated wavefront (green line) and the QAO compensated wavefront (blue line). We can see the Strehl ratio increases as the compensation degree increases, as expected.

#### 4.3. Analysis of the results

We paid attention to two different aspects of the compensation produced when we applied this procedure. On the one hand, we compared the reduction in the typical deviation of the intensity

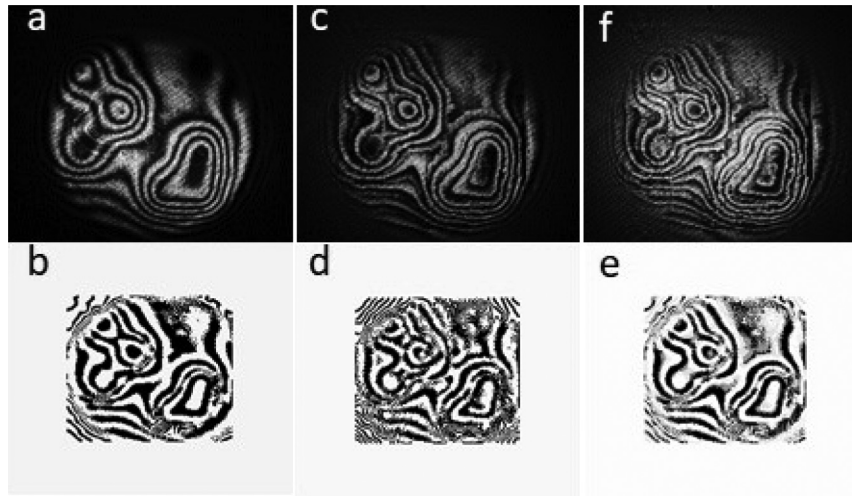


**Fig. 9.** (a) Interferogram of the distorted wavefront. (b) Binary function BF1 obtained from Fig. 9(a), (c) Interferogram of the BAO compensated wavefront, (d) Binary function BF2 obtained from Fig. 9(c), (e) Quaternary function BF1 + BF2 obtained from Fig. 9(b) + 9(d), (f) Interferogram of the QAO compensated wavefront.

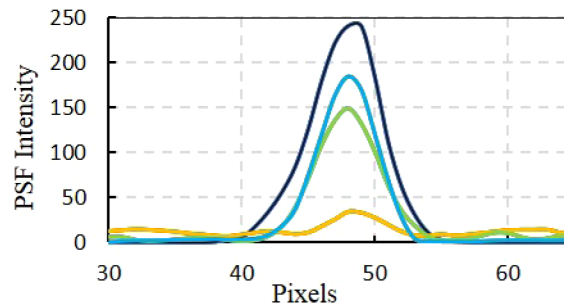


**Fig. 10.** Transverse cuts of the PSF intensity (in grey level) for the plane (black line), aberrated (yellow line), BAO compensated (green line) and QAO compensated (blue line) wavefronts.

produced in the PDI interferogram ( $\sigma_I$ ) during the compensation process. On the other hand, we measured the increase of the Strehl ratio of the compensated PSF due to the use of the binary and quaternary masks.

We first used a series of concave wavefronts with different curvatures. Concave wavefronts were corrected using first BAO and then QAO. In Table 1, we see values of the Strehl ratio and interferogram typical deviation,  $\sigma_I$ , for the aberrated, the BAO compensated and the QAO compensated wavefronts corresponding to three different curvature radii. A Strehl ratio equal to one corresponds to flat DM and zero phase SLM configuration. Strehl ratio errors and  $\sigma_I$  errors were estimated repeating the same process 10 times. Errors were around 5% for  $S$  and 2.5% for  $\sigma_I$  in all cases. Table 2 shows the same results as Table 1 for a convex wavefront series.

In general, both tables show that the Strehl increases and  $\sigma_I$  decreases as the degree of compensation grows. However, some figures require an additional comment. We can see that when the distorted wavefront is relatively flat (lowest phase value), Strehl ratios may be above the theoretical limit (0.4 for BAO and 0.8 for QAO). We consider that this result is consistent with the fact of we are taking a reference slightly affected by astigmatism as will be shown in

**Table 1. S and  $\sigma_I$  for three spherical concave wavefronts with decreasing radii**

CONCAVE	$2\pi$ Peak-to-Valley Phase		$4\pi$ Peak-to-Valley Phase		$6\pi$ Peak-to-Valley Phase	
	SR	$\sigma_I$	SR	$\sigma_I$	SR	$\sigma_I$
QAO	0.91	40	0.88	39	0.81	40
BAO	0.74	42	0.56	42	0.60	43
Ab.WF	0.14	49	0.08	48	0.06	54

**Table 2. S and  $\sigma_I$  for three spherical convex wavefronts with decreasing radii**

CONVEX	$6\pi$ Peak-to-Valley Phase		$8\pi$ Peak-to-Valley Phase		$10\pi$ Peak-to-Valley Phase	
	SR	$\sigma_I$	SR	$\sigma_I$	SR	$\sigma_I$
QAO	0.92	40	0.78	40	0.72	41
BAO	0.74	43	0.60	43	0.48	44
Ab.WF	0.08	47	0.09	47	0.06	48

Fig. 12. However, for strongly aberrated wavefronts, it is more difficult to reach that limit. This is because the number of actuators required for an effective compensation increases as the surface complexity increases.

In Table 3, we show a list of the Strehl ratio and  $\sigma_I$  values corresponding to randomly aberrated wavefronts, and the same values after BAO and QAO compensation. We see that the slightly distorted wavefront provides a high Strehl ratio prior to correction. In this case, after BAO and QAO compensation, the Strehl ratio can reach values higher than 0.8. When we have an intermediate distortion degree the Strehl ratio increases with compensation but a final Strehl of 0.74 is obtained, which is below the theoretical limit. Finally, for the case of the highly aberrated wavefront, although it starts from a Strehl ratio similar to that with intermediate distortion, both BAO and QAO provide poor compensation. This is due to the limited resolution of the SLM used in the compensation process as we commented in the QAO performance analysis section.

**Table 3. S and  $\sigma_I$  for three randomly aberrated wavefronts with increasing aberration degree**

RANDOM	Slight distortion		Intermediate distortion		High distortion	
	SR	$\sigma_I$	SR	$\sigma_I$	SR	$\sigma_I$
QAO	0.87	41	0.74	44	0.46	43
BAO	0.60	44	0.51	45	0.29	45
Ab.WF	0.19	45	0.07	48	0.06	50

These three cases were selected to show that when the wavefront variance is low, both BAO and QAO techniques may provide Strehl ratio values stated by Eq. (1). However, the technique's performance drops quickly when the compensation device (SLM or DM) does not provide sufficient resolution to compensate the high-frequency modulations involved in the description of the aberrated wavefront shape.

#### 4.4. Effect of compensation on the PSF

As a final verification, in Fig. 11 we compare the shape of the PSF series obtained during the compensation process. Figure 11(a) shows the PSF obtained when aberration is introduced. It can be seen that it suffers a little astigmatism. Figure 11(b) shows the effect of introducing the aberration named Random (Slight distortion) in Table 3. We can see that the peak energy drops significantly and a series of speckles appear around the PSF peak. When BAO compensation is applied, Fig. 11(c), not only does the energy return to the central peak but also the initial

astigmatism is also compensated. Finally, after applying QAO the PSF peak energy suffers an important increase and residual speckle is removed, Fig. 11(d). Hence, we can conclude that the experiment confirms that the BAO and QAO techniques can be successfully applied to compensate aberrated wavefronts in a simple way.

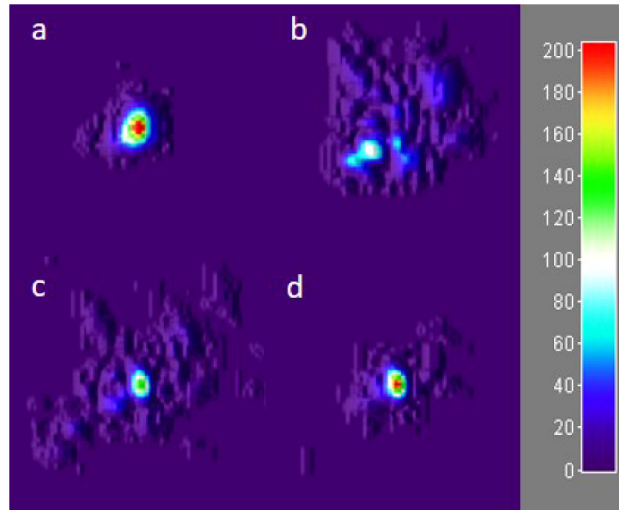


**Fig. 11.** a: Non aberrated PSF. b: Aberrated PSF. c: BAO compensated PSF and d: QAO compensated PSF.

## 5. Conclusions

We have introduced a new technique based on the quaternary compensation of distorted wavefronts. Until now, the compensation has consisted of introducing an extra binary mask with phase values 0 or  $\pi$ . We extended this technique to create a new mask with values 0 and  $\pi/2$  so that the addition of both masks creates a new quaternary mask with values 0,  $\pi/2$ ,  $\pi$  and  $3\pi/2$ . To achieve this new mask, it is only necessary to repeat the same process twice, hence no extra devices or calculations have to be introduced. It is important to remark that the key to achieving the QAO compensation is to use a PDI mask which introduces a  $\pi/2$  phase shift between aberrated and reference wavefronts. Consequently, the QAO technique has the same advantages as the BAO one, that is, we have a direct and fast phase estimation with a high wavefront sampling rate and an infinite dynamic range. Moreover, as we do not need any wavefront reconstruction processing, the time delay between detection and compensation is shortened. Since the compensating device has to be able to produce only four different phase values, it has an infinite compensating dynamic range.

From the point of view of the experimental results, we have verified that PSF Strehl ratio increases with compensation and, in some cases, the improvement is below the expected limit. However, different errors in the detection and mask creation process may affect the results. In particular, we noted that when the wavefront is affected by short-term modulations, an effective compensation could only be achieved when the number of actuators is sufficiently high.

## Funding

Ministerio de Economía y Competitividad (MINECO) (AYA2016-78773-C2-1-P).

## References

1. G.D. Love, R. Myers, A. Purvis, and R. Sharples, "A new approach to adaptive wavefront correction using a liquid crystal half-wave phase shifter," in *ICO-16 Conference on Active and Adaptive Optics* (European Southern Observatory, 1993), pp. 295–300.
2. G. D. Love, N. Andrews, P. Birch, D. Buscher, P. Doel, C. Dunlop, J. Major, R. Myers, A. Purvis, R. Sharples, A. Vick, A. Zadrozny, S. R. Restaino, and A. Glindemann, "Binary adaptive optics: atmospheric wave-front correction with a half-wave phase shifter," *Appl. Opt.* **34**(27), 6058–6066 (1995).
3. J. Osborn, R. M. Myers, and G. D. Love, "PSF halo reduction in adaptive optics using dynamic pupil masking," *Opt. Express* **17**(20), 17279–17292 (2009).
4. P. Crabtree, C. L. Woods, J. Khoury, and M. Goda, "Binary phase-only filtering for turbulence compensation in fiber-coupled free-space laser communication systems," *Appl. Opt.* **46**(34), 8335–8345 (2007).
5. F. Fatemi and M. Bashkansky, "Cold atom guidance using a binary spatial light modulator," *Opt. Express* **14**(4), 1368–1375 (2006).
6. M. Neil, M. Booth, and T. Wilson, "Dynamic wave-front generation for the characterization and testing of optical systems," *Opt. Lett.* **23**(23), 1849–1851 (1998).
7. R. N. Smartt and W. H. Steel, "Theory and application of point diffraction interferometers," *Jpn. J. Appl. Phys.* **14**(S1), 351–355 (1975).
8. E. Acosta, S. Chamadoira, and R. Blendowske, "Modified point diffraction interferometer for inspection and evaluation of ophthalmic components," *J. Opt. Soc. Am. A* **23**(3), 632–637 (2006).
9. D. Malacara, M. Servin, and Z. Malacara, *Interferogram analysis for optical testing* (Marcel Dekker, 1998).
10. M. Servin, J. L. Marroquin, and F. J. Cuevas, "Fringe-follower regularized phase tracker for demodulation of closed-fringe interferograms," *J. Opt. Soc. Am. A* **18**(3), 689–695 (2001).
11. P. M. Birch, J. Gourlay, G. D. Love, and A. Purvis, "Real-time optical aberration correction with a ferroelectric liquid-crystal spatial light modulator," *Appl. Opt.* **37**(11), 2164–2169 (1998).
12. F. Bai and C. Rao, "Experimental validation of closed-loop adaptive optics based on a self-referencing interferometer wavefront sensor and a liquid-crystal spatial light modulator," *Opt. Commun.* **283**(14), 2782–2786 (2010).
13. T. Vettenburg and A. R. Harvey, "Correction of optical phase aberrations using binary-amplitude modulation," *J. Opt. Soc. Am. A* **28**(3), 429–433 (2011).
14. C. Montero-Orille, V. Moreno, X. Prieto-Blanco, E. F. Mateo, E. Ip, J. Crespo, and J. Liñares, "Ion-exchanged glass binary phase plates for mode-division multiplexing," *Appl. Opt.* **52**(11), 2332–2339 (2013).